ACS OMEGA

Open Access

http://pubs.acs.org/journal/acsodf

Article

Prunellate A: An Unprecedented Lignan Lactone with a 6/7/6/5-Fused Tetracycle Skeleton by C-2−C-2′ and C-7−C-8′ Linkage from the Chinese Medicinal Plant *Prunella vulgaris* Inhibiting the Activation of Hepatic Stellate Cells by Targeting FXR

Xiuqin Zheng, Yi Zhang, Qian Zhang, Jia-rui Jiang, Zhu-zhen Han, Li-hua Gu,* Li-li Ding, Rui Wang,* Li Yang,* and Zheng-tao Wang

Cite This: *ACS Omega* 2025, 10, 12425−12431

Read Online

ACCESS | Metrics & More | Article Recommendations | Supporting Information

ABSTRACT: Prunellate A (**1**), an unprecedented lignan lactone bearing a 6/7/6/5 tetracyclic system with C-2−C-2′ and C-7−C-8′ single bond linkage, probably derived from the rearrangement of methyl rosmarinate (**2**), has been isolated from the medicinal plant *Prunella vulgaris*. An extensive interpretation of multispectroscopic data including HRMS, IR, 1D, and 2D NMR elucidated its structure. The stereochemical assignment was conclusively established through electronic circular dichroism (ECD) experiments. The possible biosynthetic routes for the rearrangement from **2** to **1** were deduced. The antifibrosis activity was tested according to the traditional application of raw materials. Prunellate A exhibited a significant inhibition effect against TGFβ1-induced activation on LX-2 cells by targeting the Farnesoid X Receptor (FXR). These results indicated that prunellate A has great potential for use in the treatment of liver fibrosis.

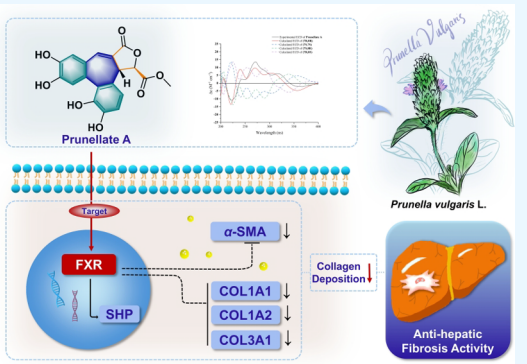

1. INTRODUCTION

Liver fibrosis is one of the processes of chronic liver disease, which involves scar tissue caused by abnormal deposition of extracellular matrix (ECM).[1] Although the process of liver fibrosis is reversible, the slow reversals are only negligible when compared with life-threatening complications.[2] Thus, delaying fibrosis and accelerating reversal is crucial in treatment.[3] Hepatic stellate cells (HSC) are closely linked to liver fibrosis and are major myofibroblast sources.[4] The pieces of evidence showed that inhibiting the activation of HSC is an effective therapeutic strategy for liver fibrosis.[4,5]

Prunella vulgaris, a medicinal plant belonging to the Lamiaceae family, grows in temperate zones and elevated tropical ecosystems across multiple continents, including Eurasian territories, northwestern African highlands, and North American bioregions.[6,7] In traditional Chinese usage, *P. vulgaris* is considered to transfer to the liver meridian and could be used to protect the liver.[8] Modern pharmacological research verified that *P. vulgaris* can demonstrate suppression of cellular invasive and migratory capabilities across hepatocellular carcinoma models.[9] The aqueous extract alleviates hepatic fibrosis,[10] and the methanol extract possesses highly significant hepatoprotective activity[11] as well. Recently, many phytochemicals like triterpenoids and their saponins, phenolic acids, flavonoids, and polysaccharides have been found in *P. vulgaris* , exhibiting anti-inflammatory properties, lowering blood lipids and pressure, anticancer activity, and anti-aging.[12,13] However, few monomeric components with hepatoprotective activity have been reported,[14] drawing attention to further phytochemical research. To date, plant lignans have various biological activities, including liver protection. Lignans from multiple plants showed their hepatoprotective activities significantly, such as the lignans isolated from the fruits of *Leonurus japonicus*,[15] the fruits of *Hippophae rhamnoides*,[16] and the roots of *Kadsura longipedunculata*.[17]

In our studies, a novel lignan named prunellate A bearing a 6/7/6/5 four-membered cycle system has been isolated. For the first time, an unprecedented 2−2′,7−8′ linked Biphenyl cycloheptene skeleton has been found in natural products. To the best of our knowledge, cyclolignans are less distributed in nature. Most cyclolignans possess a 2−2′, 8−8′ linked biphenyl cyclooctene skeleton, which is found solely in individual plants of the *Schisandra* family and the *Umbelliferae* family.[18] However, 2,2′-cyclo-7,8′-neolignan has not been discovered

Received: December 26, 2024
Revised: March 5, 2025
Accepted: March 12, 2025
Published: March 20, 2025

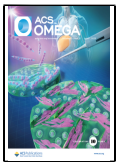

yet, not to mention within the Lamiaceae family. Thus, the skeleton of **1** was classified as a new type- "dibenzocycloheptadiene," which could not be added to current lignan classification: "dibenzocyclooctadiene," "arylnaphthalene and aryltetralin," "dibenzylbutane, dibenzylbutyrolactol and dibenzylbutyrolactone," "furofuran derivatives," and "furan derivatives."[19] Therefore, according to the efficacy of the original medicinal materials and the structure−activity relationship of the compounds, the inhibitory effect of prunellate A on HSC activation was evaluated and its potential mechanism was studied in this paper. Unsurprisingly, prunellate A showed a good hepatoprotective potential.

2. RESULTS AND DISCUSSION

Prunellate A (**1**) was obtained as a green oil (MeOH). Its molecular formula, $C_{19}H_{14}O_8$, was deduced by negative HR-ESI-MS at m/z 369.0616 $[M-H]^-$ (calcd for $C_{19}H_{13}O_8$ m/z 369.0610), indicating 13 degrees of unsaturation. Infrared spectroscopic characteristic vibrations at 3347 and 1741 cm^{-1} correspond to the hydroxy group and carbonyl functionalities, respectively. The ^1H NMR spectrum showed signals for a pair of *ortho*-aromatic protons [δ_H 6.81 (1H, d, J = 8.32 Hz), H-5; δ_H 6.84 (1H, d, J = 8.32 Hz), H-6], a pair of *para*- aromatic protons [δ_H 7.39 (1H, s), H-3′; δ_H 6.94 (1H, s), H-6′], a β-olefinic proton located at an α,β-unsaturated carbonyl moiety at [δ_H 7.37 (1H, d, J = 1.93 Hz), H-7′], a deshielded oxygenated methine hydrogen at δ_H 5.79 (1H, d, J = 2.42 Hz, H-8), and a group of oxymethyl proton signal at δ_H 3.72 (3H, s, H_3-10). The ^{13}C NMR spectrum of **1** showed 19 carbon resonances (Table 1), which could be sorted into two ester carbonyl carbon (δ_C 170.2, C-9; δ_C 172.5, C-9′), 14 aromatic/olefinic carbon (CH × 5, C × 9), one typical oxymethyl (δ_C 58.5, C-10), together with two methines (one oxygenated at δ_C 75.6) signals with the aid of DEPT-135 experiment.

The planar structure of **1** was demonstrated by a comprehensive interpretation of its 2D NMR data. In the HMBC spectrum, the correlations of H-3′/C-4′, C-5′, and C-1′; H-6′/C-2′, C-5′, C-1′, and C-7′; H-7′/ C-1′, C-2′, and C-6′ indicated the presence of a 1,2,4,5-substituted benzene ring (ring A′) unit. In the same way, another 1,2,3,4-substituted benzene ring (ring A) unit was disclosed according to HMBC correlations of H-5 to C-3 and C-1, of H-6 to C-2 and C-4. The key HMBC correlation between H-3′ and C-2 confirmed the linkage of the two benzene rings described above by C-2 and C-2′. Furthermore, the HMBC spectrum gave the correlations from H-7 to C-7′, C-8′, and C-9′, which affirmed the connection between C-7 and C-8′. Therefore, a biphenyl cycloheptene nucleus was assigned without a doubt. The NOE correlations of H-6′/H-7′ and H-6/H-7 can also be a testimony to the above judgment. In addition, the $^1H-^1H$ COSY cross peak of H-7/H-8, together with the HMBC correlation of H-8/C-9′, constructed a five-membered lactone ring (ring C). This judgment is also consistent with the characteristic chemical shift observed for H-8 (δ_H 5.79) due to the shielded effect caused simultaneously by the vicinal acyl oxygen and carboxyl groups. This observation may provide a reference for the compounds containing the 5-oxotetrahydrofuran-2-carboxylate segment. Finally, the HMBC correlation of H_3-10 to C-9 assigned the position of the oxymethyl group. Thus, the gross structure of **1** was established.

1 has two chiral centers at C-7 and C-8. To solve its stereochemistry, ECD calculation was availed. The absolute configuration of **1** was disclosed by ECD calculation based on time-dependent density functional theory (TD-DFT) for all four conformers. As a result, the experimental ECD curve of **1** was in good agreement with the calculated ECD curve of 7*R*,8*R*-**1**. Consequently, the structure of **1** was elucidated as shown in Figure 1, and named prunellate A. Prunellate A is a new lignan containing a unique 2−2′,7−8′ linked Biphenyl cycloheptene skeleton. Up to now, this is the first example of a carbon skeleton in the natural kingdom. We propose using the name "dibenzocycloheptadiene" for this new lignan skeleton type.

Table 1. NMR Spectroscopic Data of Prunellate A (δ in ppm)[a]

position	δ_H, mult, intrgt (J)	δ_C (mult)
1		133.4 (C)
2		125.2 (C)
3		146.0 (C)
4		145.4 (C)
5	6.81 (1H, d, J = 8.32 Hz)	112.3 (CH)
6	6.84 (1H, d, J = 8.32 Hz)	114.9 (CH)
7	3.46 (1H, t, J = 2.30 Hz)	46.4 (CH)
8	5.79 (1H, d, J = 2.42 Hz)	75.6 (CH)
9		172.5 (C)
10	3.73 (3H, s)	53.5 (CH_3)
1′		130.5 (C)
2′		128.9 (C)
3′	7.39 (1H, s)	121.5 (CH)
4′		145.9 (C)
5′		146.7 (C)
6′	6.94 (1H, s)	117.1 (CH)
7′	7.37 (1H, d, J = 1.94 Hz)	136.2 (CH)
8′		129.7 (C)
9′		170.2 (C)

[a] ^1H (400 MHz) and ^{13}C (100 MHz) NMR data for compound in MeOD-d_4.

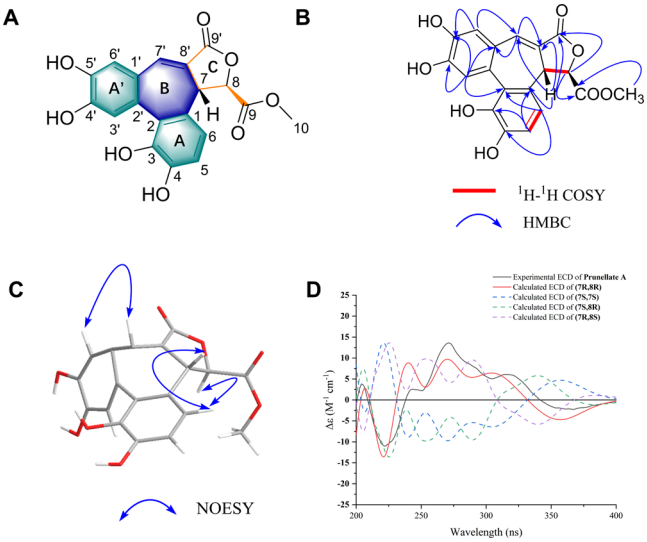

Figure 1. Structure Identification of Prunellate A. (A) Structure of Prunellate A. (B,C) Key $^1H-^1H$ COSY, HMBC, and NOESY correlations of Prunellate A. (D) Calculated and experimental ECD spectra of Prunellate A.

https://doi.org/10.1021/acsomega.4c11609
ACS Omega 2025, 10, 12425−12431

Scheme 1. Proposed Biogenesis Pathway of Prunellate A

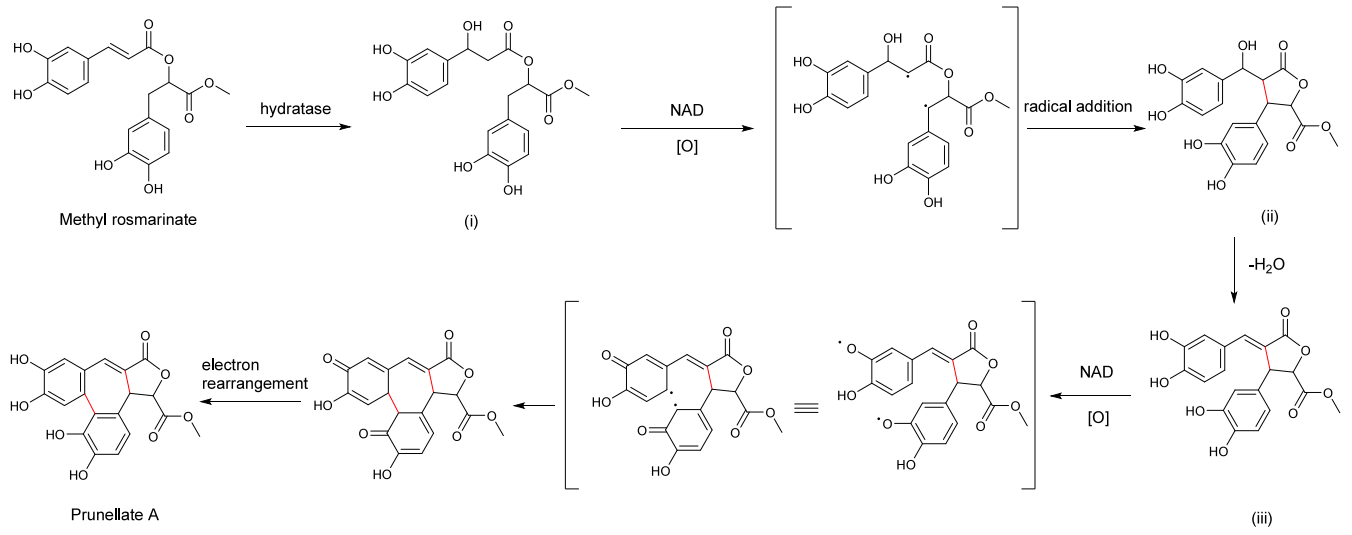

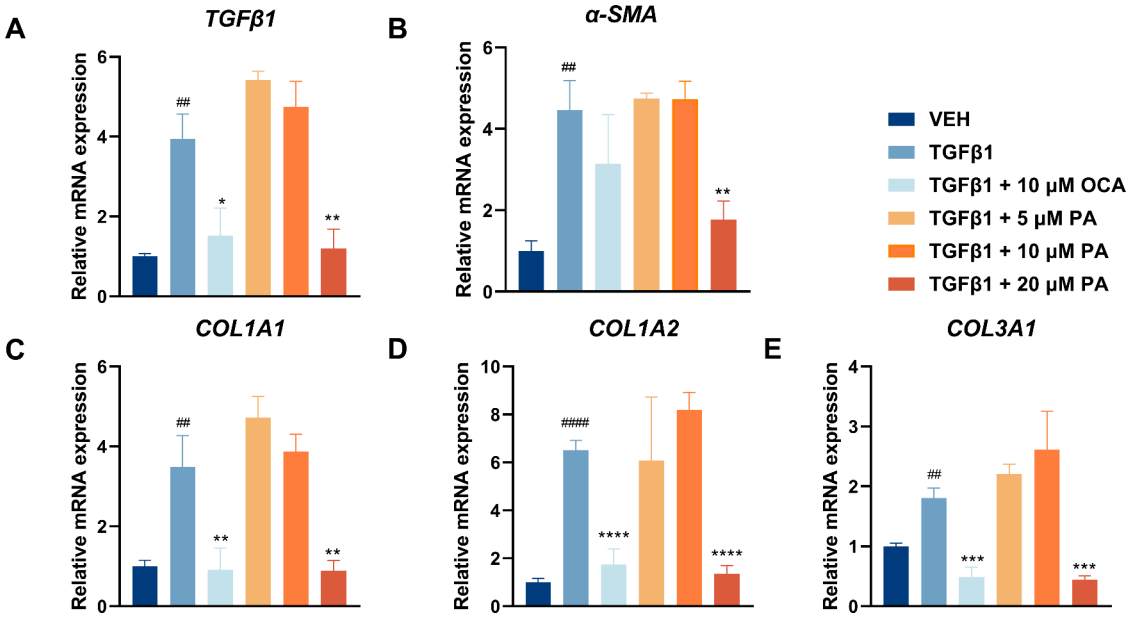

Figure 2. Effects of Prunellate A (PA) on the mRNA expression of liver fibrosis markers in LX-2. (A) *TGFβ1*, (B) *α-SMA*, (C) *COL1A1*, (D) *COL1A2*, (E) *COL1A3* genes were determined by real-time PCR. Data represent means ±SD of three independent experiments. ##$p < 0.01$, ####$p < 0.0001$ vs VEH, *$p < 0.05$, **$p < 0.01$, ***$p < 0.001$, ****$p < 0.0001$ vs TGFβ1.

The proposed biogenetic origin of Prunellate A can be plausibly traced to methyl rosmarinate (**2**), a natural phenolic compound in many plants belonging to the Lamiaceae family[20] (Scheme 1). First, methyl rosmarinate formed midbody (i) under the action of hydratase. Next, dehydrocoenzyme NAD catalyzed (i) the production of a diradical intermediate at C-7 and C-8′, which formed its radical addition product (ii) and subsequent product (iii) after dehydration. A similar enzymatic reaction resulted in the formation of a single bond between C-2 and C-2′. Ultimately, electron rearrangement occurred to establish prunellate A with a unique 2−2′,7−8′ linked biphenyl cycloheptene skeleton.

To evaluate the biopharmacological properties of prunellate A (PA), the cellular toxicity profile was assessed in LX-2 cells through standardized cell counting kit-8 (CCK-8) assays. The experimental data demonstrated that the tested compound was not cytotoxic.

LX-2 cells treated with transforming growth factor β (TGFβ1) have been extensively used as a liver fibrosis model in vitro. In this model, the expression of hepatic fibrosis factor, especially α-Smooth Muscle Actin (α-SMA) would be increased when stimulated by TGFβ1. Obecholic acid (OCA) was used as a positive agent. The real-time polymerase chain reaction (RT-qPCR) method was formed to evaluate the treatment effect of PA in LX-2 cells induced by TGFβ1. The results demonstrated that PA could decrease the mRNA level of fibrosis cytokines, including *TGFβ1*, *α-SMA*, *COL1A1*, *COL1A2*, and *COL3A1*, which indicated that this compound was effective in ameliorating the activation of HSC (Figure 2). To explore further mechanisms, we designed a series of experiments.

The structure of PA was similar to deoxyschizandrin, which has been reported as a farnesoid X receptor (FXR) agonist.[21] FXR, a ligand-activated transcription factor, is mainly ex-

https://doi.org/10.1021/acsomega.4c11609
ACS Omega 2025, 10, 12425−12431

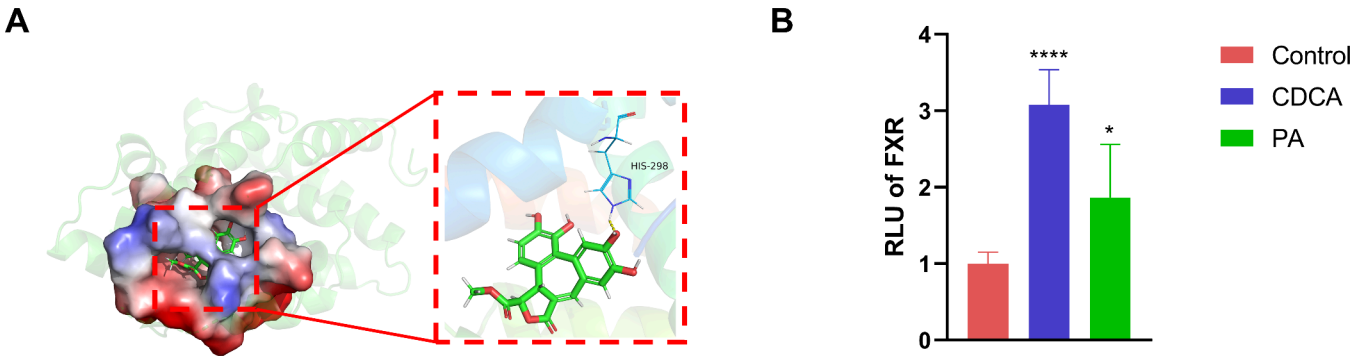

Figure 3. Interaction between prunellate A (PA) and FXR. (A) Putative binding mode of prunellate A (PA) with FXR. (B) Luciferase assay of FXR activation. HEK293T cells transfected with the plasmids of FXR, RXR-α, ECRE, and Renilla were incubated with Prunellate A (PA) (20 μM) and CDCA (10 μM), respectively. Data represent means ± SD of three independent experiments. *p < 0.05, **p < 0.01, ***p < 0.001, ****p < 0.0001 vs Control.

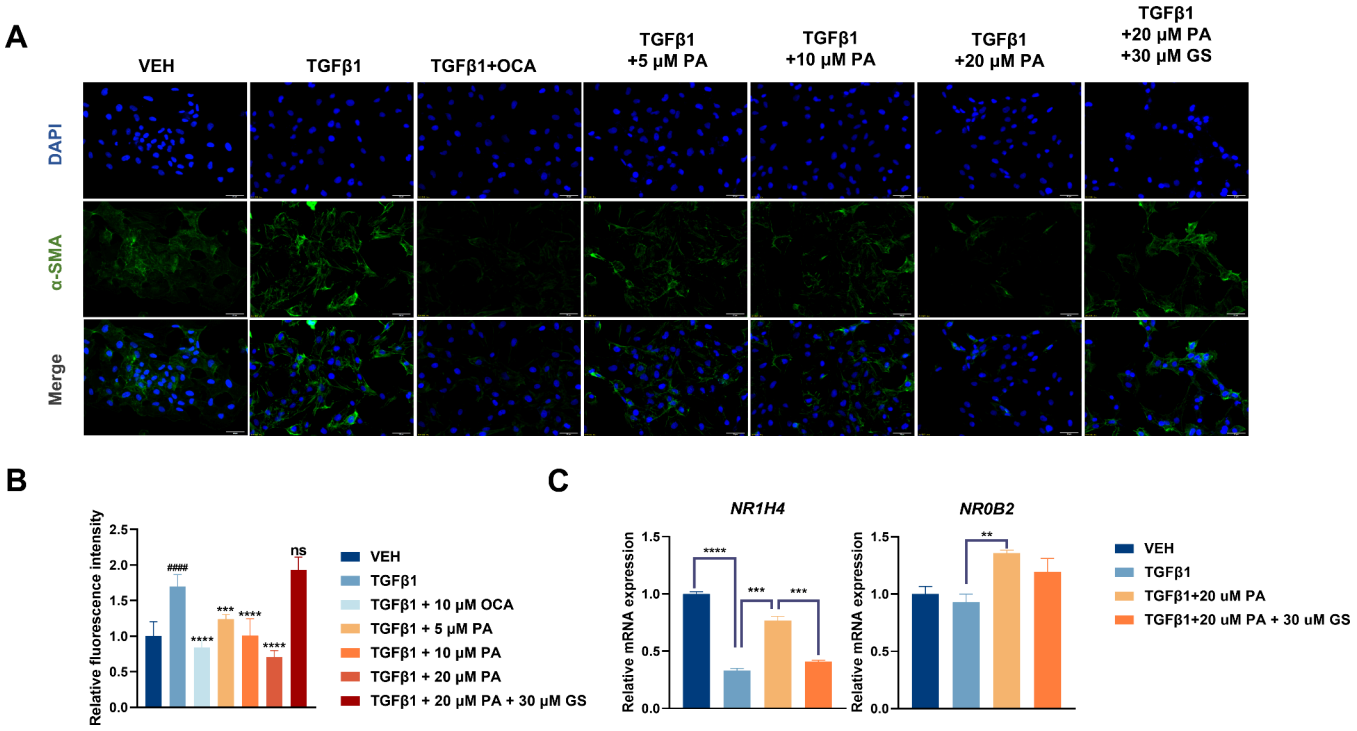

Figure 4. PA reduces the expression of the TGFβ1-induced liver fibrosis marker(α-SMA) by targeting FXR in LX-2. (A) α-SMA was stained green and DAPI in blue. Scale bar: 50 μm. (B) Quantitative analysis of fluorescence intensity as an indication of α-SMA levels. Data represent means ± SD of three independent experiments. ##p < 0.01, ####p < 0.0001 vs VEH, *p < 0.05, **p < 0.01, ***p < 0.001, ****p < 0.0001 vs TGFβ1. (C) Effects of PA on mRNA expression of FXR and SHP. Data represent means ± SD of three independent experiments. **p < 0.01, ***p < 0.001, ****p < 0.0001.

pressed in the liver, kidney, and intestine.[22] In recent years, research on the mechanism of FXR in liver injury has extensively attracted the attention of scholars. FXR activation can alleviate pathological hepatic conditions, such as non-alcoholic fatty liver disease, liver fibrosis,[23] etc. To reveal whether there is a correlation between the pharmacodynamics of PA and FXR activation, we designed molecular docking and luciferase assays to investigate the agonist effect of FXR in vitro. Molecular docking can determine the interaction forces and exact binding sites between proteins and small molecules. Figure 3A shows the combined feature information on PA and FXR. The binding energy of PA and FXR is −8.821 kcal/mol, and the oxygen at the C-4′hydroxyl group has a hydrogen bonding force with HIS-298, with a hydrogen bond length of 2.3 Å, indicating that the binding has occurred spontaneously. In the luciferase assay (Figure 3B), the relative luciferase activity of the intervention group given PA was increased significantly compared with the control group. All evidence suggests that PA is an agonist of FXR.

Furthermore, according to the results of RT-qPCR and fluorescent luciferase assay, we conducted a cellular immunofluorescence experiment to explore whether PA can inhibit the activation of HSC by activating FXR. The fluorescence intensity of α-SMA, which reflects the degree of activation of HSC was significantly enhanced after being induced by TGFβ1. The intensity was decreased after being treated with PA, indicating this compound can reduce the expression of α-SMA in a dose-dependent manner. After the administration of

https://doi.org/10.1021/acsomega.4c11609
ACS Omega 2025, 10, 12425−12431

FXR inhibitors (Guggulsterone), the fluorescence intensity of α-SMA will not be reduced after being treated with PA Figure 4A. The fluorescence intensity of the blank group and drug treatment group was quantified, and the results are shown in Figure 4B. Meanwhile, the downstream gene expression of FXR was detected. The results showed that PA can stimulate FXR and reverse the expression of FXR mRNA inhibited by TGFβ1 in vitro, and the effect was weakened after adding FXR inhibitors (Figure 4C). This indicates that Prunellate A inhibits the activation of HSC by activating FXR, which has a potential therapeutic effect on liver fibrosis.

3. CONCLUSIONS

In conclusion, this study discovered a new skeleton compound named Prunellate A belonging to the dibenzocycloheptadiene class from the spikes of the medicinal herb *P. vulgaris*. By analyzing NMR and mass spectrometry data, the planar structure of the compound has been elucidated. The absolute configuration was determined using quantum chemical calculations. This new skeleton molecule enriches research on *P. vulgaris*. It is noteworthy that this compound exhibits significant activity in inhibiting the activation of hepatic stellate cells. Molecular docking and luciferase assays were utilized to identify their biological effects by targeting FXR. This study provides a foundation for further in vivo studies and could potentially lead to new agents for treating liver fibrosis disease. Furthermore, it suggests that previous studies may have overlooked the potential of *P. vulgaris* in treating liver disease, and this discovery offers a new avenue for its development and utilization in this regard. Meanwhile, we recognized that in vitro biological activity studies are far from sufficient. It is essential to further investigate the biosynthetic and chemical synthetic pathways of this compound based on experimental evidence in the future. This will provide the necessary raw materials for animal experiments and allow for continued exploration of its pharmacological effects and possible mechanisms against hepatic fibrosis in animal models, thereby laying the foundation for clinical applications.

4. EXPERIMENTAL SECTION

4.1. General Experimental Procedures. Initial fractionation was executed using silica gel (200−300 mesh, Qingdao Marine Chemical Co., Ltd., China). Subsequent purification stages employed a reverse-phase medium-pressure liquid chromatography system (Buchi Labortechnik AG, Flawil, Switzerland) coupled with YMC ODS reversed-phase columns (50 μm, YMC Co., Ltd., Kyoto, Japan), and Sephadex LH-20 (GE Healthcare Bio-Sciences AB, Uppsala, Sweden). Final compound isolation was accomplished through semi-HPLC on a chuangxintongheng LC3000 system, featuring a UV-100D detector at 210 nm, and an Xbridge C_{18} ODS column (250 × 20 mm, 5 μm). Chiroptical properties were characterized by using an OLIS DSM1000 spectrophotometer. TLC and preparative TLC (PTLC) analyses utilized $HSGF_{254}$ plates (Yantai Huanghai Silica Gel Development Co., Ltd., China), and compound visualization was achieved through a UV lamp at 254 nm and chemical revelation via spraying with 10% H_2SO_4 in EtOH, followed by thermal activation.

The NMR spectra were utilized in a Bruker AV III 400 MHz spectrometer (Bruker Corporation, Karlsruhe, France), with TMS serving as the internal reference. High-resolution mass spectrometric characterization was achieved through a Q-TOF mass spectrometer (Waters, Massachusetts, USA). Optical rotation determinations were conducted on an Autopol IV automated polarimeter (Rudolph, New Jersey, USA). Infrared spectra acquisition was employed with a PerkinElmer Spectrum 100 FTIR system with a universal attenuated total reflectance accessory (UATR), covering the range 4000−600 cm^{-1}.

4.2. Plant Materials. Desiccated infructescence from *P. vulgaris* L. was obtained in Anhui province's Huangshan region in June 2020. Origin verification was conducted by Professor Li-Hong Wu following standard botanical identification protocols. A representative voucher (No. XKC20200612) has been permanently archived in the medicinal plant repository at the Shanghai University of Traditional Chinese Medicine's Institute of Chinese Materia Medica for future reference.

4.3. Extraction and Isolation. The desiccated infructescence of *P. vulgaris* L. underwent mechanical fragmentation followed by sequential solvent extraction processes. Initial extraction employed 95% ethanol through reflux (2 × 150 L, 2 h each time) and underwent second extraction with 70% ethanol (1 × 120 L, 2 h each time). Following vacuum-assisted evaporation of the extracts at reduced pressure, 2.2 kg of crude material was obtained. This was then extracted with petroleum, CH_2Cl_2, and EtOAc, respectively.

The EtOAc extract (300 g) underwent chromatographic fraction using an MCI column (Mitsubishi Chemical, MCI GEL CHP 20P) eluting with 80%, and 100% MeOH to yield two subfractions, A and B. Fraction A was subjected to a silica gel (3 kg, 200−300 mesh) column, employing dichloromethane-MeOH (from 100:1 to 5:1), to afford 12 subfractions A1−A12 under TLC monitoring. A systematic isolation strategy was implemented for fraction A6, involving three sequential purification steps: RP-MPLC with 30% MeOH, molecular sieving through Sephadex LH-20 in methanol, and final purification via semipreparative HPLC (ACN-H_2O 36:64 v/v). This multistep process yielded compound 1 (11 mg). The same processing of fraction A7 was RP-MPLC with MeOH-H_2O (30%), and Sephadex LH-20 (MeOH) to obtain compound **2** (826 mg).

(**1**) Green oil. [α]20 D + 187.34 (*c*0.1, CH_3OH); IR vmax 3347, 2922, 1741, 1278, 1197, 1014, 799 cm^{-1}; ^1H and ^{13}C NMR spectroscopic data see Tables 1; negative ion HR-ESI-MS *m*/*z* 369.0616 $[M - H]^-$ (calcd 369.0610 for $C_{19}H_{13}O_8$).

(**2**) Brown oil. (CH_3OH) ^1H NMR spectrum (400 MHz, CD_3OD, δ, ppm, *J*/Hz): 7.56 (1H, d, *J* = 15.9, H-7), 7.05 (1H, d, *J* = 1.8, H-2′), 6.78 (1H, d, *J* = 8.1, H-5′), 6.57 (1H, dd, *J* = 8.1, 1.8, H-6′), 6.70 (1H, d, *J* = 8.4, H-5), 6.71 (1H, d, *J* = 2.0, H-2), 6.96 (1H, dd, *J* = 8.4, 2.0, H-6), 6.27 (1H, d, *J* = 15.9, H-8), 5.19 (1H, dd, *J* = 7.4, 5.3, H-8′), 3.02 (2H, m, H-7′), 3.71 (3H, s, H-OMe). ^{13}C NMR spectrum (100 MHz, CD_3OD, δ, ppm): 127.7(C-1), 117.7 (C-2), 150.0 (C-3), 147.0 (C-4), 116.5 (C-5), 123.4 (C-6), 148.1 (C-7), 114.3 (C-8), 168.5 (C-9), 128.9(C-1′), 115.4(C-2′), 146.4(C-3′), 145.5(C-4′), 116.7(C-5′), 145.6(C-4′), 38.0(C-7′), 74.8(C-8′), 172.3(C-9′), 52.8(-OMe).

4.4. ECD Calculation. Structure analysis of the target molecule was initiated through conformational sampling, employing the OPLS3 molecular mechanics force field for energy calculations. Molecular configurations exhibiting relative energies below a 3.0 kcal/mol threshold were prioritized for subsequent quantum mechanical refinement. Density functional theory (DFT) optimizations were performed using the B3LYP hybrid functional with the 6-

https://doi.org/10.1021/acsomega.4c11609
ACS Omega 2025, 10, 12425−12431

311G(d,p) basis set in Gaussian 09. The Boltzmann distribution ratio of each conformation was obtained according to the energy of each conformation after optimization. Then, conformations with a Boltzmann distribution over 1% were chosen for ECD calculations. The 60 excited states of each conformation were calculated by the TD-DFT method at the B3LYP/6-311G(d,p) level. The ECD spectra of the compounds were fitted by using SpecDis1.70 software and compared with the experimental spectra.

4.5. Molecular Docking. The crystallographic coordinates of FXR (PDB code: 1OSV) were sourced from the RCSB Protein Data Bank (https://www.rcsb.org/). Initial structural refinement involved the excision of the B polypeptide chain and all nonessential molecular components, including coenzymes and heteroatomic species, from the primary data set. The prepared protein file and PA files are imported into Maestro (version 11.1) from Schrodinger's computational technology. After that, Glide (Schrodinger, LLC, New York) for virtual screening was used to semiflexibly dock the processed compound structure and protein structure, and the results were visualized using PyMOL. The docking score calculated by the software represents the affinity between the protein and the ligand, and the lower the score, the higher the stability of the protein−ligand complex. Repeated experiments with other crystal structures (PDB ID: 3BEJ and 6HL1) gave results similar to those in this paper.

4.6. Cell Culture. HEK293T cells were purchased from the Cell Bank of Shanghai Institute of Biological Sciences, Chinese Academy of Sciences (Shanghai, China). LX-2 cells were purchased from Procell Life Science & Technology Co., Ltd. The cells were propagated in a DMEM medium enriched with 10% FBS and 1% penicillin/streptomycin antibiotic cocktail. Cell maintenance was performed in a temperature-regulated incubator (37 °C) within a controlled humidity environment containing 5% CO_2.

4.7. Transfection and Reporter Gene Assays. HEK293T cells were maintained in DMEM enriched with 10% FBS and cotransfected with EcRE-Luc, phFXR, phRXR, and β-galactosidase at the ratio of 10:2.5:2.5:1 by the Lipofectamine 2000 procedure (Invitrogen Life Technologies, Carlsbad, CA, USA). After 8 h, cells were treated with CDCA (10 μM) or Prunellate A (20 μM) for 24 h. Following 24 h incubation, cells were harvested, and the luciferase activity was analyzed using a luciferase reporter assay system, adhering strictly to the manufacturer's standardized operational procedures (Promega, Madison, WI, USA). Each transfection was performed in triplicate and repeated at least three times.

4.8. Quantitative PCR (qPCR) Assay. The total RNA of LX-2 cells was conducted by utilizing a Fastagen RNA purification solution under manufacturer-specified procedures. The concentration of RNA was assessed through a spectrophotometer at 260 and 280 nm absorbance. cDNA synthesis was achieved via an Evo M-MLV Master Mix, implementing recommended thermal cycling parameters. Quantitative PCR was performed using a SYBR Green qPCR Master Mix, and each sample was independently tested three times. Gene expression normalization employed GAPDH as an endogenous control, with fold-change calculations performed through comparative threshold cycle ($2^{-\Delta\Delta CT}$) analysis. All primer sequences used are listed in Table S1.

4.9. Immunofluorescence Assay. LX-2 cells were placed onto glass coverslips and cultured for 24 h before being treated with TGFβ1, OCA, and Prunellate A. After 24 h of treatment, the coverslips were rinsed with PBS 3 times, then immobilized with 4% paraformaldehyde for 20 min, rendered permeable with 0.5% Triton X-100 in PBS for 15 min, and obstructed with 0.2% BSA, 0.2% donkey serum, and 0.03% Triton X-100 in PBS for 1h. Next, the cells were stained with primary antibody α-SMA (ABclonal, A17910) at 4 °C overnight, rinsed with PBS 3 times, and stained with 488-conjugated Goat Anti-Rabbit IgG (H+L) (ABclonal, AS053) labeled secondary antibody for 1 h at room temperature. After incubation, the coverslips were rinsed with PBS and the fluorescence quenching sealing solution containing DAPI. The coverslips were then fixed with adhesive. Finally, fluorescence microscopic images were captured by using epifluorescence microscopy.

■ ASSOCIATED CONTENT

Data Availability Statement

The data underlying this study are available in the published article and its Supporting Information.

Supporting Information

The Supporting Information is available free of charge at https://pubs.acs.org/doi/10.1021/acsomega.4c11609.

NMR data, HR-ESI-MS, and IR spectrum of compound **1**; general experimental procedures (SI 2.1); plant material (SI 2.2); extraction and isolation methods (SI 2.3); ECD calculation (SI 2.4, Table S1); cell culture method (SI 2.5); transfection and reporter gene assays (SI 2.6); quantitative PCR (qPCR) assay (SI 2.7); primers for qPCR (Table S2); and immunofluorescence assay (SI 2.8) (PDF)

■ AUTHOR INFORMATION

Corresponding Authors

Li-hua Gu − *Institute of Chinese Materia Medica, Shanghai University of Traditional Chinese Medicine, Shanghai 201203, P. R. China*; orcid.org/0000-0003-4924-7904; Email: lhgu@shutcm.edu.cn

Rui Wang − *School of Pharmacy, Shanghai University of Traditional Chinese Medicine, Shanghai 201203, P. R. China*; Email: ellewang@163.com

Li Yang − *Institute of Chinese Materia Medica, Shanghai University of Traditional Chinese Medicine, Shanghai 201203, P. R. China*; Email: yl7@shutcm.edu.cn

Authors

Xiuqin Zheng − *School of Pharmacy, Shanghai University of Traditional Chinese Medicine, Shanghai 201203, P. R. China*

Yi Zhang − *Institute of Chinese Materia Medica, Shanghai University of Traditional Chinese Medicine, Shanghai 201203, P. R. China*

Qian Zhang − *Institute of Chinese Materia Medica, Shanghai University of Traditional Chinese Medicine, Shanghai 201203, P. R. China*

Jia-rui Jiang − *Institute of Chinese Materia Medica, Shanghai University of Traditional Chinese Medicine, Shanghai 201203, P. R. China*

Zhu-zhen Han − *Institute of Chinese Materia Medica, Shanghai University of Traditional Chinese Medicine, Shanghai 201203, P. R. China*

Li-li Ding − *Institute of Chinese Materia Medica, Shanghai University of Traditional Chinese Medicine, Shanghai 201203, P. R. China*

https://doi.org/10.1021/acsomega.4c11609
ACS Omega 2025, 10, 12425−12431

Zheng-tao Wang − *Institute of Chinese Materia Medica, Shanghai University of Traditional Chinese Medicine, Shanghai 201203, P. R. China;* orcid.org/0000-0003-2797-4625

Complete contact information is available at: https://pubs.acs.org/10.1021/acsomega.4c11609

Notes

The authors declare no competing financial interest.

■ ACKNOWLEDGMENTS

This study was financially supported by a project from the Shanghai Natural Science Fund (No. 19ZR1457200) and a grant from the Shanghai Program project from the Shanghai University of Traditional Chinese Medicine (No. A1-GY20-306-02-03).

■ REFERENCES

(1) Parola, M.; Pinzani, M. Liver fibrosis: Pathophysiology, pathogenetic targets and clinical issues. *Mol. Aspects Med.* **2019**, *65*, 37−55.

(2) Roehlen, N.; Crouchet, E.; Baumert, T. F. Liver Fibrosis: Mechanistic Concepts and Therapeutic Perspectives. *Cells* **2020**, *9* (4), 875.

(3) Kisseleva, T.; Brenner, D. Molecular and cellular mechanisms of liver fibrosis and its regression. *Nat. Rev. Gastroenterol Hepatol* **2021**, *18* (3), 151−166.

(4) Tsuchida, T.; Friedman, S. L. Mechanisms of hepatic stellate cell activation. *Nat. Rev. Gastroenterol Hepatol* **2017**, *14* (7), 397−411.

(5) Higashi, T.; Friedman, S. L.; Hoshida, Y. Hepatic stellate cells as key target in liver fibrosis. *Adv. Drug Deliv Rev.* **2017**, *121*, 27−42.

(6) Bai, Y.; Xia, B.; Xie, W.; Zhou, Y.; Xie, J.; Li, H.; Liao, D.; Lin, L.; Li, C. Phytochemistry and pharmacological activities of the genus Prunella. *Food Chem.* **2016**, *204*, 483−496.

(7) Zheng, X. Q.; Song, L. X.; Han, Z. Z.; Yang, Y. B.; Zhang, Y.; Gu, L. H.; Yang, L.; Chou, G. X.; Wang, Z. T. Pentacyclic triterpenoids from spikes of Prunella vulgaris L. with thyroid tumour cell cytostatic bioactivities. *Nat. Prod Res.* **2023**, *37* (9), 1518−1526.

(8) Commission, C. P. *China Pharmacopoeia, 2020*. China Medical Science Press: Beijing, 2020.

(9) Su, Y. C.; Lin, I. H.; Siao, Y. M.; Liu, C. J.; Yeh, C. C. Modulation of the Tumor Metastatic Microenvironment and Multiple Signal Pathways by Prunella vulgaris in Human Hepatocellular Carcinoma. *Am. J. Chin Med.* **2016**, *44* (4), 835−849.

(10) Hu, Y. X.; Yu, C. H.; Wu, F.; Yu, W. Y.; Zhong, Y. S.; Ying, H. Z.; Yu, B. Antihepatofibrotic Effects of Aqueous Extract of Prunella vulgaris on Carbon Tetrachloride-Induced Hepatic Fibrosis in Rats. *Planta Med.* **2016**, *82* (1−2), 97−105.

(11) Ahmad, G.; Masoodi, M. H.; Tabassum, N.; Mir, S. A.; Iqbal, M. J. Invivo hepatoprotective potential of extracts obtained from floral spikes of Prunella vulgaris L. *J. Ayurveda Integr Med.* **2020**, *11* (4), 502−507.

(12) Li, P.; Lv, X.; Wang, J.; Zhang, C.; Zhao, J.; Yang, Y. Research on the anti-ageing mechanism of Prunella vulgaris L. *Sci. Rep* **2023**, *13* (1), 12398.

(13) Wang, S. J.; Wang, X. H.; Dai, Y. Y.; Ma, M. H.; Rahman, K.; Nian, H.; Zhang, H. Prunella vulgaris: A Comprehensive Review of Chemical Constituents, Pharmacological Effects and Clinical Applications. *Curr. Pharm. Des* **2019**, *25* (3), 359−369.

(14) Cao, Y.; Tan, X.; Al Chnani, A. A.; Li, P.; Shi, Z.; Feng, H.; Sun, L.; Xia, Q.; Yang, X.; Duan, Y.; Guo, Y.; Chen, G.; Qi, C.; Zhang, Y. Bioassay-Guided Isolation of an Abetiane-Type Diterpenoid from Prunella vulgaris That Protects against Concanavalin A-Induced Autoimmune Hepatitis. *J. Nat. Prod* **2021**, *84* (8), 2189−2199.

(15) Tian, Z. H.; Liu, F.; Peng, F.; He, Y. L.; Shu, H. Z.; Lin, S.; Chen, J. F.; Peng, C.; Xiong, L. New lignans from the fruits of Leonurus japonicus and their hepatoprotective activities. *Bioorg Chem.* **2021**, *115*, No. 105252.

(16) Ma, Q.; Guan, Y.; Sang, Z.; Dong, J.; Wei, R. Isolation and characterization of auronlignan derivatives with hepatoprotective and hypolipidemic activities from the fruits of Hippophae rhamnoides L. *Food Funct* **2022**, *13* (14), 7750−7761.

(17) Shao, S. Y.; Qi, X. Z.; Sun, H.; Li, S. Hepatoprotective lignans and triterpenoids from the roots of Kadsura longipedunculata. *Fitoterapia* **2020**, *142*, No. 104487.

(18) Jafernik, K.; Motyka, S.; Calina, D.; Sharifi-Rad, J.; Szopa, A. Comprehensive review of dibenzocyclooctadiene lignans from the Schisandra genus: anticancer potential, mechanistic insights and future prospects in oncology. *Chin. Med.* **2024**, *19* (1), 17.

(19) Teponno, R. B.; Kusari, S.; Spiteller, M. Recent advances in research on lignans and neolignans. *Nat. Prod Rep* **2016**, *33* (9), 1044−1092.

(20) Liu, R.; Heiss, E. H.; Waltenberger, B.; Blazevic, T.; Schachner, D.; Jiang, B.; Krystof, V.; Liu, W.; Schwaiger, S.; Pena-Rodriguez, L. M.; Breuss, J. M.; Stuppner, H.; Dirsch, V. M.; Atanasov, A. G. Constituents of Mediterranean Spices Counteracting Vascular Smooth Muscle Cell Proliferation: Identification and Characterization of Rosmarinic Acid Methyl Ester as a Novel Inhibitor. *Mol. Nutr. Food Res.* **2018**, *62* (7), No. e1700860.

(21) Gu, M.; Feng, Y.; Chen, Y.; Fan, S.; Huang, C. Deoxyschizandrin ameliorates obesity and non-alcoholic fatty liver disease: Involvement of dual Farnesyl X receptor/G protein-coupled bile acid receptor 1 activation and leptin sensitization. *Phytother Res.* **2023**, *37* (7), 2771−2786.

(22) Tian, S. Y.; Chen, S. M.; Pan, C. X.; Li, Y. FXR: structures, biology, and drug development for NASH and fibrosis diseases. *Acta Pharmacol Sin* **2022**, *43* (5), 1120−1132.

(23) Zhou, J.; Cui, S.; He, Q.; Guo, Y.; Pan, X.; Zhang, P.; Huang, N.; Ge, C.; Wang, G.; Gonzalez, F. J.; Wang, H.; Hao, H. SUMOylation inhibitors synergize with FXR agonists in combating liver fibrosis. *Nat. Commun.* **2020**, *11* (1), 240.